optica

Polarization-sensitive reconstruction of transient local THz fields at dielectric interfaces

Kay Waltar,[1] Johannes Haase,[2] Rui Pan,[3] Torsten Golz,[3] Pavel Kliuiev,[1] Michael Weinl,[4]
Matthias Schreck,[4] Saša Bajt,[3] Nikola Stojanovic,[3] Jeroen A. van Bokhoven,[2,5]
Matthias Hengsberger,[1] Jürg Osterwalder,[1] and Luca Castiglioni[1,*]

[1]*Physics Department, University of Zurich, Zurich, Switzerland*
[2]*Laboratory for Catalysis and Sustainable Chemistry, Paul Scherrer Institute, Villigen, Switzerland*
[3]*Deutsches Elektronen-Synchrotron-DESY, Hamburg, Germany*
[4]*Institut für Physik, Universität Augsburg, D-86135 Augsburg, Germany*
[5]*Institute for Chemical and Bioengineering, ETH Zurich, Zurich, Switzerland*
*Corresponding author: castiglioni@physik.uzh.ch

Intense THz fields can be used to excite specific low-frequency modes in condensed matter or drive confined currents in nano-structured arrays, paving the way for a new class of optoelectronic devices. The long wavelength enables spatially confined field enhancement due to interaction with metallic structures and interference effects at dielectric interfaces. We use THz photoelectron streaking for the polarization-sensitive reconstruction of all electric field components at dielectric and metallic interfaces. This is realized in a THz/x-ray pump–probe experiment where x-ray emitted photoelectrons probe the effective THz field in close surface proximity. We observe distinct differences in the THz response of a nano-structured Pt thin film and a Pt(111) bulk crystal, in particular for the parallel field component. Simulations of the nanoscale spatial field modulation at metallic islands on the thin film provide design parameters for different sensitivity regimes with respect to local fields. © 2019 Optical Society of America under the terms of the OSA Open Access Publishing Agreement

https://doi.org/10.1364/OPTICA.6.001431

1. INTRODUCTION

The increasing availability of sources of strong ultrashort THz pulses in recent years has enabled new types of experiments where the electric field is used to drive and control dynamic processes [1,2]. THz fields can be used to induce lightwave-driven currents in a topological surface band [3]; to stimulate atomic motion in adsorbed molecules, thereby controlling their reactivity [4]; or to electrically write antiferromagnetic memory devices [5]. In many cases, large field amplitudes and/or narrow-bandwidth radiation are required which can, for instance, be generated in free-electron-laser (FEL) undulators [6]. Another approach to locally increase the field amplitude is through the application of metamaterial array structures in which localized charge carriers can resonate with the incoming radiation and hence increase the electric field in surface plasmon polaritons [7–9]. In addition, isolated metallic elements such as split-ring resonators, nano-slits, and dipolar antennas enable localized strong field enhancement [10–13]. Atoms and molecules placed in close vicinity to these nanostructures can be studied under the influence of the enhanced fields, given a suitable probing technique.

Both polarization and amplitude of the exciting THz field are essential parameters in such experiments. The THz near field can be accessed by only a few non-intrusive methods. Electro-optic sampling (EOS) and imaging have been used to measure the electric near-field enhancement along dipolar Au antennas on

LiNbO$_3$ waveguides [14]. The spatial resolution is limited by the optical diffraction limit, and the temporal resolution by the duration of the optical probe pulse. However, this method relies on specific THz propagation media as substrates [15,16]. The THz field is subject to not only local enhancement, but also to modifications due to interaction with dielectric or metallic media. This is particularly true at and near interfaces, where the effective fields result from a superposition of incoming and reflected waves. Near metallic structures, screening charges can substantially distort the field both in terms of amplitude and polarization. In this work, we address the question of how photoelectron streaking [17–20] can be used for spatiotemporal characterization of effective THz fields near solid–vacuum interfaces at different length scales.

Figure 1(a) shows a schematic overview of the streaking experiment. The interaction of the THz pulse with metallic or dielectric media leads to a transient field grating at the interface due to superposition of incoming and reflected waves. Photoelectrons emitted by a time-delayed x-ray pulse with initial momentum $\vec{p}_0$ are accelerated in the local field and subject to a momentum change $\Delta\vec{p}$ [19]. Using an angle-resolved electron analyzer, distinctive modifications of the momentary momentum distribution can directly be recorded [Fig. 1(b)]. A field vector along the detection axis of the analyzer leads to a change of the kinetic energy
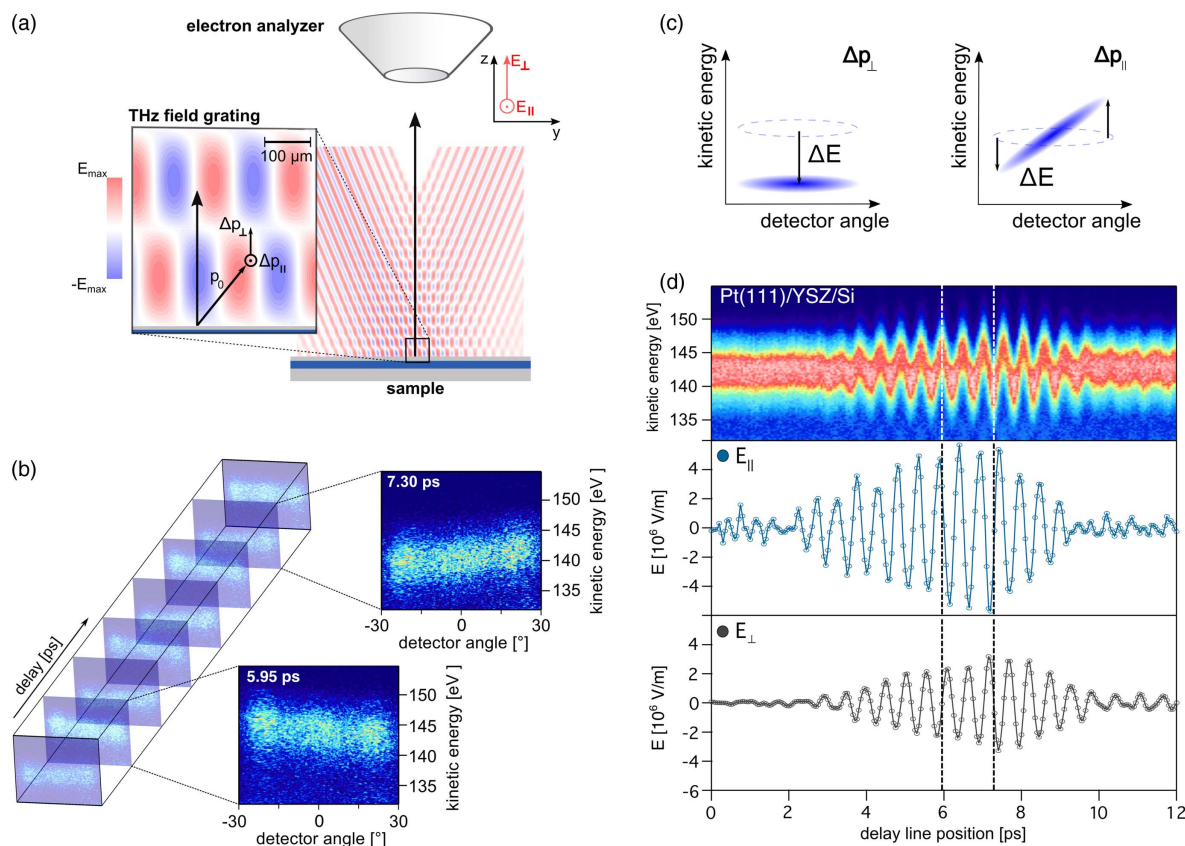
Fig. 1. Terahertz streaking scheme and polarization-sensitive pulse reconstruction. (a) Superposition of incoming and reflected parts of the THz pulse generate a complex field grating above the sample surface. The magnified inset shows possible momentum modifications of emitted electrons due to interaction with the E-field. (b) Stack of raw detector data of the Pt $5d$ valence level at different THz/x-ray delays, showing the effect of tilting and shifting of the electron momentum distribution. (c) Schematics of the individual effects of the perpendicular (left) and parallel (right) field components on the momentum distribution. (d) Angle-integrated delay trace of the thin-film sample (top) and reconstructed field components parallel (center) and perpendicular (bottom) to the sample surface. Dashed lines indicate the delays of the detector images in (b).

[Fig. 1(c), left], whereas a field perpendicular to the detection axis leads to an antisymmetric energy shift, resulting in an apparent tilting of the momentum distribution [Fig. 1(c), right]. This momentum change can be related to the time-dependent amplitude and polarization direction of the effective THz near field along the emission trajectory. Figure 1(d) shows an experimental streaking trace together with the reconstructed electric field components. The polarization-sensitive reconstruction of all field components was previously developed in our group and verified based on Monte Carlo simulations [21]. The spatial and temporal resolution is determined by the footprint of the focused x-ray beam at the surface, the initial electron momentum, and the duration of the x-ray pulse, which is usually a small fraction of the THz period.

To assess the applicability of this method, we compare reconstructed field components of a THz pulse on a bulk Pt(111) single crystal and a thin metallic film made up of individual nanoscale Pt(111) islands grown on a dielectric layer. A particular focus is put on the parallel electric field component that is expected to be well screened at THz frequencies due to the high density and fast response of free charge carriers at late transition metal surfaces. Frequency-domain electromagnetic simulations of the near-field screening response of Pt islands are compared with our experimental results in order to assess the relative contributions of near- and far-field effects to the streaking data.

2. METHODS

A. Experimental Setup

Our THz/x-ray pump–probe experiment was set up at the THz beamline [22] of the FLASH free electron laser [Fig. 2(a); see Supplement 1 for details]. Both soft x-ray and THz pulses are generated by the same electron bunch in dedicated undulators, and are thus naturally synchronized. The 151 eV third harmonic of the x-ray pulse was used as probe beam and focused on the sample with a multi-layer mirror. A detailed view of the measurement geometry is given in Fig. 2(b). The s-polarized THz pulse was focused nearly collinearly using a 30° off-axis parabolic mirror adjacent to the sample. Photoelectrons are collected over a wide acceptance angle ($\pm30°$) in a hemispherical analyzer, and dispersed in energy and angle before detection [see Fig. 1(b) for typical raw detector images].

B. Electric Field Reconstruction

Scanning the delay between THz and x-ray pulses leads to modification of the photoelectron momenta that can be recorded as streaking spectrograms. We display only the angle-integrated traces [Fig. 1(d), top], but the full electron momentum information is stored for each time step [Fig. 1(b)]. This enables the reconstruction of both parallel and perpendicular components of the THz field on the sample surface using our previously published approach [21].
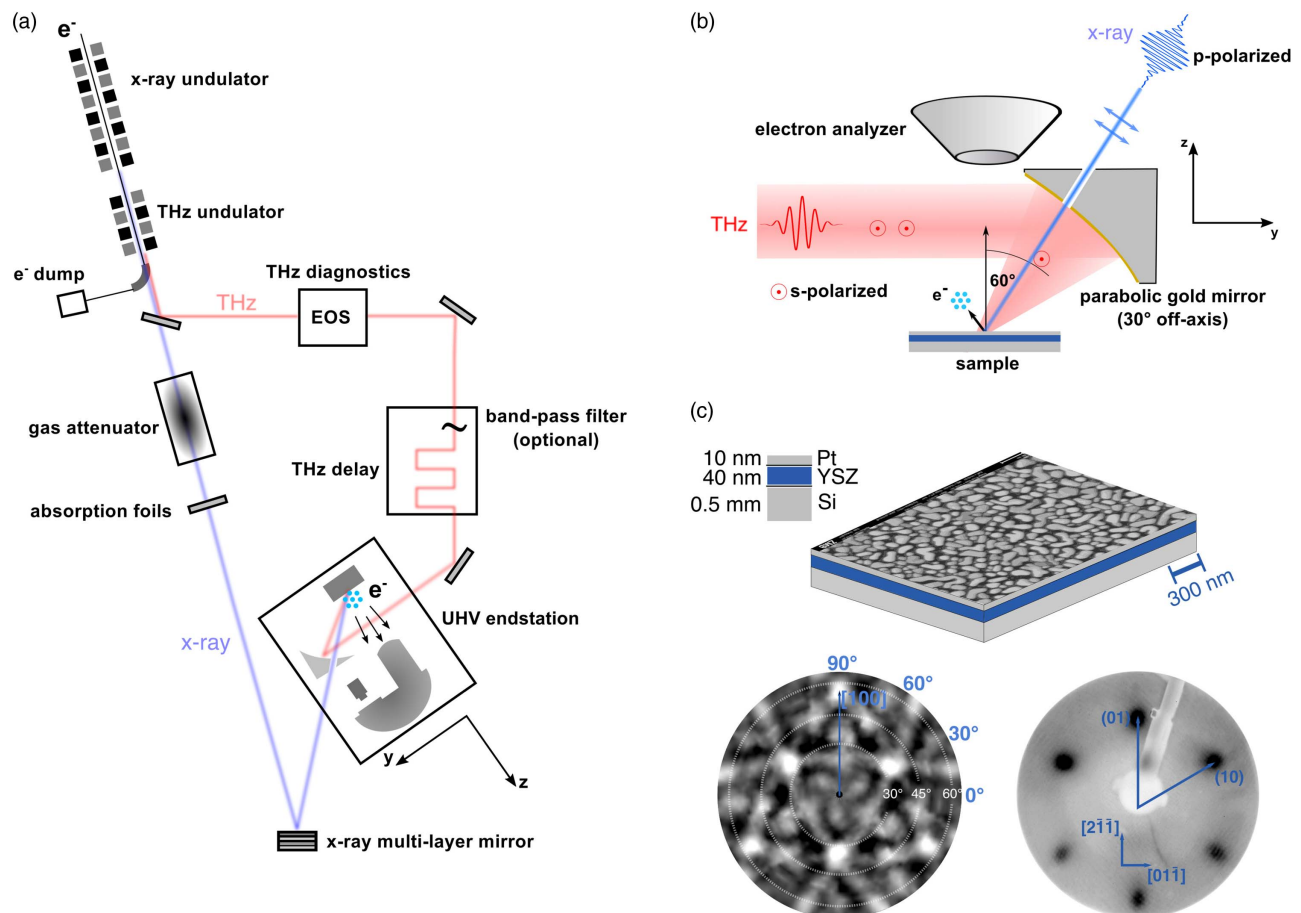
Fig. 2. Experimental setup of the THz/x-ray pump–probe experiment and thin-film sample characterization. (a) Schematics of the experimental setup. The x-ray beam path is set up in a back-reflection geometry via a multi-layer mirror. (b) Measurement geometry inside the UHV chamber. The THz beam is tightly focused onto the sample by an off-axis parabolic mirror. The x-ray light enters the interaction region from the back side of the same mirror through a small hole. Polarizations are as indicated. Photoemitted electrons are detected by a hemispherical electron analyzer. (c) Schematic of the thin-film sample with an SEM image showing the island-like Pt surface texture; bottom images show XPD map of the Pt 4f core level (left) and LEED image of the thin film (right).

In brief, the detector images are divided into angular channels, and we look for energy shifts of spectral features in each channel. Perpendicular and parallel field components lead to distinctive shift patterns [see Fig. 1(c)] that let us calculate the individual field components at each time step (see Supplement 1). We note that given the particular experimental setup and type of electron analyzer, only the parallel field component along the angle-dispersive axis of the analyzer (x-axis) can be reconstructed. This does not preclude a full 3D reconstruction of all field components using a different experimental setup.
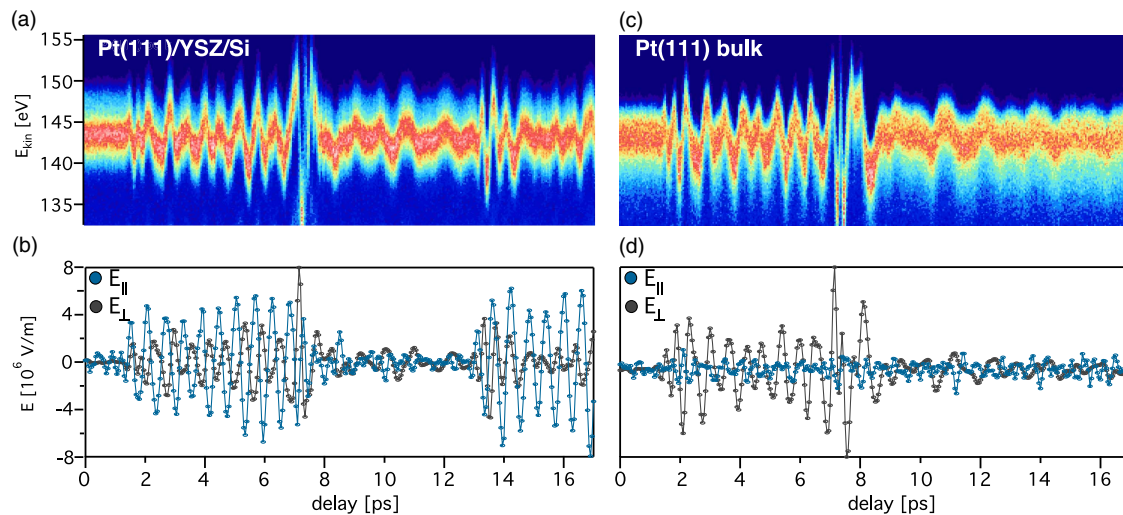
C. Samples

We employed two different types of samples to explore the capabilities and limitations of the reconstruction approach. Besides the Pt(111) bulk single crystal, where we expect total reflection of the THz pulse, we also studied a Pt thin film on a dielectric substrate that is largely transparent for THz radiation [Fig. 2(c); see Supplement 1 for details]. The scanning electron microscope (SEM) image reveals nanometer-sized Pt islands on the yttria-stabilized zirconia (YSZ) interlayer on a Si wafer. The crystallinity and (111) orientation of the Pt islands is verified by x-ray photoelectron diffraction (XPD) and low-energy electron diffraction (LEED).

3. RESULTS

A. Reconstructed Electric Field Components at Pt(111) Bulk and Thin-Film Surfaces

Typical angle-integrated streaking spectrograms for a 2 THz pulse with a duration of ∼5 ps are shown in Fig. 3. In case of the Pt(111) thin film [Fig. 3(a)], we see two pulses starting at 1.6 and 13.3 ps. The reconstruction [Fig. 3(b)] reveals parallel and perpendicular field components of comparable magnitude in the first pulse. The amplitude of the parallel component in the second pulse is ∼40% larger than in the first pulse. The overall temporal shape of the parallel component is similar in both pulses. In case of the Pt(111) bulk sample, we observe only the first pulse [Fig. 3(c)]. The reconstructed perpendicular component [Fig. 3(d)] is comparable to the first pulse on the thin film, but the parallel component is vanishing within the noise level of about $0.5 \cdot 10^6$ Vm^{-1}.

The absence of the parallel component of the electric field on the bulk sample can be explained by efficient screening of the external field due to the fast ($\omega_{\mathrm{THz}} \ll \omega_{\mathrm{p}}$, i.e., the plasma frequency) reaction of free charge carriers inside the metal. The perpendicular component does not vanish in accordance with Fresnel's equations. The presence of a persisting perpendicular component, despite an undulator-generated s-polarized THz pulse, can be explained by a

Fig. 3. THz streaking of the Pt(111) valence level and reconstructed field components. (a) Angle-integrated delay trace of the Pt(111) valence level of the thin-film sample. (b) The reconstructed electric field components parallel (blue) and perpendicular (grey) to the sample surface are presented below. (c–d) Same as in (a) and (b), respectively, but for Pt(111) bulk sample.

slight misalignment of the off-axis parabolic focusing mirror (see Supplement 1). If this mirror were the only source of the perpendicular component, the parallel and perpendicular field components would be either in phase or 180° out of phase, depending on the definition of the detector angle axis. This is indeed the case in the central part of the reconstructed first pulse in Fig. 3(b). At the rising and falling edges of the pulse, additional contributions to the perpendicular component can be observed. They become apparent by the changing relative phase shift between parallel and perpendicular field components and originate from transition undulator radiation [23] and edge radiation [24,25]. Their polarizations differ from the actual undulator radiation, i.e., linear *s*-polarized light. The existence of two pulses on the thin-film sample is due to (i) direct reflection of the incoming THz light at the vacuum/YSZ and YSZ/Si interfaces and (ii) back-reflection of the transmitted part of the incoming light at the Mo sample holder onto which the thin film is mounted. The first reconstructed pulse is a superposition of the incoming and directly reflected THz pulse, which generates a field grating. The second pulse, which starts 11.7 ps after the first, is due to back-reflection at the Mo sample holder. This explains the larger reconstructed amplitude of the parallel component in the second pulse since this transmitted part of the pulse is not subject to formation of a transient grating and the associated field reduction. The delay corresponds to the time it takes the THz light to travel the optical path within the multilayered thin film twice. Using Fresnel's equations and the experimentally determined amplitude of the parallel component in the second pulse, the amplitude of the incoming and directly reflected THz light can be determined. Assuming a metallic thin film which is transparent to the THz, the field amplitude of the incoming light is determined to be $1.7 \cdot 10^7$ Vm^{-1}; the field amplitude of the directly reflected light $-1.3 \cdot 10^7$ Vm^{-1} (see Supplement 1). This corresponds to a net amplitude of the parallel component of the field grating at the interface of $4 \cdot 10^6$ Vm^{-1}, which in turn is about the value of the first pulse reconstructed in Fig. 3(a). The initial assumption of a transparent thin metallic layer, expected for a film made of small, individual metallic islands [26], is therefore consistent with the experimental results.

B. Near-Field Effects at Nanometer-Sized Metallic Islands

In order to test the effect of additional field components in proximity to individual Pt islands, electromagnetic simulations have been performed (see Supplement 1). In Figure 4(a), the effect of a normal-incidence THz field on a 200 nm wide and 10 nm high ellipsoidal island is simulated. The total field component perpendicular to the vacuum/YSZ interface is shown on the left. The free charges on the isolated metallic islands react to the applied external field on a timescale much shorter than the period of the driving THz field. In a quasi-static picture, the free charges immediately polarize the islands along the direction of the electric field vector by electrostatic induction. The resulting charge surplus at the boundary of the island generates a perpendicular field component which penetrates far across the metallic island surface and reverses its direction at the center [Fig. 4(b), solid blue] due to charges of opposite sign at opposing edges.

The effect of the electrostatic induction on the parallel component is shown in the right part of Fig. 4(a). The induced charges generate an additional field component which enhances the total parallel field just at the island edges. The line profiles [Fig. 4(b)] at two different sampling heights above the island surface (P1 at 1 nm, P2 at 100 nm) further demonstrate the localized nature of the induced field enhancement; 100 nm above the island surfaces, the modification of the field is already negligible.

Figure 4(c) presents the same situation as before but for a *p*-polarized THz pulse with 60° incidence angle. Here, the driving THz field has components parallel and perpendicular to the surface. The effect on the total field amplitude is qualitatively the same as in the normal incidence case [Fig. 4(a)], but with reduced enhancement due to the initial distribution of the electric field amplitude into both components with the initial power flow set equal in all simulations. Figure 4(d) shows the lateral profile of the electric field components. In all simulated cases, the parallel electric field component is screened in close proximity to the island surface (P1). At distances farther away than 100 nm (P2), the field distribution resembles the situation of the THz pulse, only interacting with the
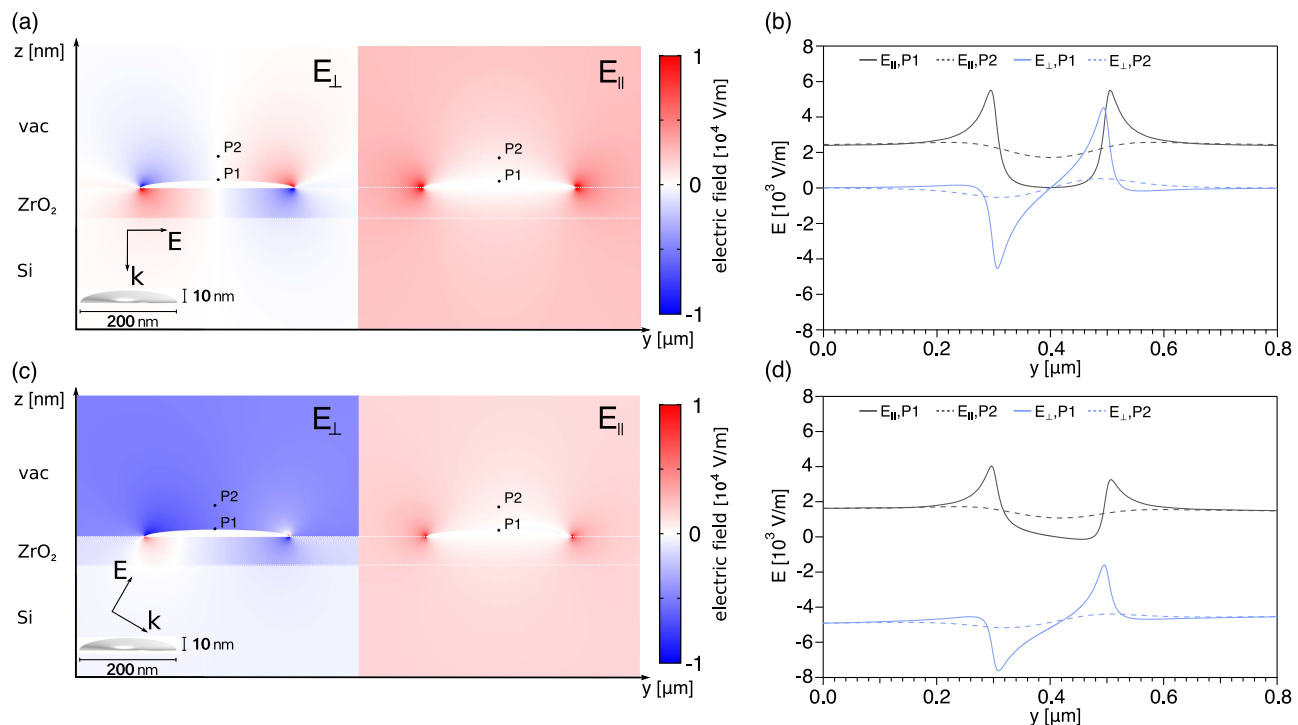
Fig. 4. Electric field simulations of THz light incident on nanometer-sized metallic islands. (a) Total electric field components perpendicular (left) and parallel (right) to the metallic island at a fixed phase of the external driving field. The vectors $\vec{E}$ and $\vec{k}$ indicate polarization and direction, respectively, of the incoming 2 THz light. Here, light is incident perpendicular to the surface at an incidence angle of 0°. (b) Line profiles of the parallel (black) and perpendicular (blue) electric field components at two heights above the island surface marked as P1 (1 nm, solid) and P2 (100 nm, dashed). (c) Same as in (a) but with an oblique angle of incidence of 60° and p-polarized light. (d) Line profiles of the electric field components from the simulation in (c). P1 and P2 are defined as in (b).

dielectric interface of vacuum and YSZ/Si(111), with almost no additional field components generated at the metal islands.

The almost complete screening of the parallel field in close proximity (<10 nm) of the metallic islands does not seem to affect the reconstructed field components from the streaking data [Figs. 3(a)–3(b)]. This can be understood by taking the finite initial momentum of the electron into account that leads to sampling of the electric field at different locations along the electron trajectory while quivering in the transient THz grating, thus leading to a spatial averaging. The distance travelled by the electron, $d_e = \Delta t \sqrt{2E_{kin}/m_e}$, corresponds to 4.26 μm during one optical cycle (Δt) with our experimental parameters (2.0 THz, 143 eV electron kinetic energy). The first 100 nm, i.e., the length-scale of metallic-island-induced near-field effects, are traversed within 14 fs. Therefore, the photoelectrons sense in essence the transient field grating due to the dielectric interfaces, which explains the presence of the reconstructed parallel component on the thin-film sample. The experimentally determined amplitudes are consistent with the model of a THz transparent metallic layer, and are also in agreement with a model presented in a recent review [27], where the authors distinguish different sensitivity regimes for the field reconstruction based on the electron velocity and the optical cycle of the driving field [28]. Given our specific parameters of high initial electron velocity and long period of the THz field, we are in the regime that is not sensitive for the enhanced near-field.

4. DISCUSSION AND PERSPECTIVES

We record time-dependent changes in the photoelectron momentum distributions to reconstruct transient THz field components in close proximity to metallic and dielectric surfaces. The method is applied to data from a FEL photoelectron streaking experiment where reconstructed field components on a bulk Pt(111) crystal are compared to those on the surface of a Pt thin film. Distinct differences in the reconstructed fields on the Pt thin-film sample and the Pt(111) bulk crystal confirm the sensitivity to the effective local field at the interfaces. The accuracy of the method is further verified by the quantitative agreement between reconstructed and simulated field amplitudes of the back-reflected pulse that was refracted and reflected at five interfaces overall. The reconstruction shows a vanishing parallel field component on the bulk crystal, as predicted by electromagnetic theory, and the presence of a perpendicular component which originates from parasitic undulator radiation and a slight tilt of the focusing mirror. In case of the thin-film sample, the simulated field modifications due to electrostatic charge induction on the small Pt-islands predict a local screening response that is comparable to the bulk crystal. The strong parallel component in the reconstruction of the experimental data must thus be attributed to a geometrical sampling effect. Namely at chosen experimental parameters (2 THz frequency and 151 eV x-ray photon energy), the high initial momentum of the photoelectrons leads to a fairly long travel range of several μm during one optical cycle of the THz pulse, resulting in an averaging of the field over this distance.

However, the overall method of field reconstruction by photoelectron momentum modification can readily be extended to probe local electric fields if appropriate kinetic energies and pulse durations are chosen. The axial resolution is given by the initial electron momentum and the THz pulse duration and frequency. If access to the nanometer-scale near-field components is desired, the initial electron kinetic energy must be reduced to <10 eV by

choosing an appropriate probe photon energy. A higher THz frequency or reduction of the pulse duration further increases the axial resolution. In essence, the parameters must be chosen such that the electron spends a significant fraction of the duration of the optical cycle in the near-field enhanced region. The lateral resolution is primarily governed by the probe pulse spot size. Sub-100 nm resolution was recently achieved in photoemission experiments using Fresnel zone plates [29]. In conjunction with powerful, full-field electron momentum microscopes [30], efficient full 3D reconstruction of the polarization information with high spatial resolution can be achieved in the near future. Finally, the chemical sensitivity of photoelectron-based field characterization (i.e., selection of an element-specific photoemission line) gives access to an additional control parameter, in particular if devices fabricated from different chemical elements are to be probed.

Disclosures. The authors declare no conflicts of interest.

REFERENCES

1. H. A. Hafez, X. Chai, A. Ibrahim, S. Mondal, D. Férachou, X. Ropagnol, and T. Ozaki, "Intense terahertz radiation and their applications," J. Opt. **18**, 093004 (2016).
2. P. Hamm, M. Meuwly, S. L. Johnson, P. Beaud, and U. Staub, "Perspective: THz-driven nuclear dynamics from solids to molecules," Struct. Dyn. **4**, 061601 (2017).
3. J. Reimann, S. Schlauderer, C. P. Schmid, F. Langer, S. Baierl, K. A. Kokh, O. E. Tereshchenko, A. Kimura, C. Lange, J. Güdde, U. Höfer, and R. Huber, "Subcycle observation of lightwave-driven dirac currents in a topological surface band," Nature **562**, 396–400 (2018).
4. J. L. LaRue, T. Katayama, A. Lindenberg, A. S. Fisher, H. Öström, A. Nilsson, and H. Ogasawara, "THz-pulse-induced selective catalytic CO oxidation on Ru," Phys. Rev. Lett. **115**, 036103 (2015).
5. K. Olejnk, T. Seifert, Z. Kašpar, V. Novák, P. Wadley, R. P. Campion, M. Baumgartner, P. Gambardella, P. Němec, J. Wunderlich, J. Sinova, P. Kužel, M. Müller, T. Kampfrath, and T. Jungwirth, "Terahertz electrical writing speed in an antiferromagnetic memory," Sci. Adv. **4**, eaar3566 (2018).
6. N. Stojanovic and M. Drescher, "Accelerator- and laser-based sources of high-field terahertz pulses," J. Phys. B **46**, 192001 (2013).
7. F. Wang and Y. R. Shen, "General properties of local plasmons in metal nanostructures," Phys. Rev. Lett. **97**, 206806 (2006).
8. B. Luk'yanchuk, N. I. Zheludev, S. A. Maier, N. J. Halas, P. Nordlander, H. Giessen, and C. T. Chong, "The fano resonance in plasmonic nanostructures and metamaterials," Nat. Mater. **9**, 707EP (2010).
9. E. Hendry, F. J. Garcia-Vidal, L. Martin-Moreno, J. G. Rivas, M. Bonn, A. P. Hibbins, and M. J. Lockyear, "Optical control over surface-plasmon-polariton-assisted THz transmission through a slit aperture," Phys. Rev. Lett. **100**, 123901 (2008).
10. Y. Takakura, "Optical resonance in a narrow slit in a thick metallic screen," Phys. Rev. Lett. **86**, 5601–5603 (2001).
11. H. Fischer and O. J. F. Martin, "Engineering the optical response of plasmonic nanoantennas," Opt. Express **16**, 9144–9154 (2008).
12. K. Ueno, S. Nozawa, and H. Misawa, "Surface-enhanced terahertz spectroscopy using gold rod structures resonant with terahertz waves," Opt. Express **23**, 28584–28592 (2015).
13. L. Razzari, A. Toma, M. Shalaby, M. Clerici, R. P. Zaccaria, C. Liberale, S. Marras, I. A. I. Al-Naib, G. Das, F. D. Angelis, M. Peccianti, A. Falqui, T. Ozaki, R. Morandotti, and E. D. Fabrizio, "Extremely large extinction efficiency and field enhancement in terahertz resonant dipole nanoantennas," Opt. Express **19**, 26088–26094 (2011).
14. C. A. Werley, K. Fan, A. C. Strikwerda, S. M. Teo, X. Zhang, R. D. Averitt, and K. A. Nelson, "Time-resolved imaging of near-fields in THz antennas and direct quantitative measurement of field enhancements," Opt. Express **20**, 8551–8567 (2012).
15. Q. Wu, C. A. Werley, K.-H. Lin, A. Dorn, M. G. Bawendi, and K. A. Nelson, "Quantitative phase contrast imaging of THz electric fields in a dielectric waveguide," Opt. Express **17**, 9219–9225 (2009).
16. C. A. Werley, Q. Wu, K.-H. Lin, C. R. Tait, A. Dorn, and K. A. Nelson, "Comparison of phase-sensitive imaging techniques for studying terahertz waves in structured LiNbO3," J. Opt. Soc. Am. B **27**, 2350–2359 (2010).
17. J. Itatani, F. Quéré, G. L. Yudin, M. Y. Ivanov, F. Krausz, and P. B. Corkum, "Attosecond streak camera," Phys. Rev. Lett. **88**, 173903 (2002).
18. U. Frühling, M. Wieland, M. Gensch, T. Gebert, B. Schütte, M. Krikunova, R. Kalms, F. Budzyn, O. Grimm, J. Rossbach, E. Plönjes, and M. Drescher, "Single-shot terahertz-field-driven x-ray streak camera," Nat. Photonics **3**, 523–528 (2009).
19. L. Castiglioni, D. Leuenberger, M. Greif, and M. Hengsberger, "Attosecond transversal streaking to probe electron dynamics at surfaces," in *Multiphoton Processes and Attosecond Physics*, K. Yamanouchi and M. Katsumi, eds. (Springer, 2012), pp. 365–368.
20. I. Grguraš, A. R. Maier, C. Behrens, T. Mazza, T. J. Kelly, P. Radcliffe, S. Düsterer, A. K. Kazansky, N. M. Kabachnik, T. Tschentscher, J. T. Costello, M. Meyer, M. C. Hoffmann, H. Schlarb, and A. L. Cavalieri, "Ultrafast x-ray pulse characterization at free-electron lasers," Nat. Photonics **6**, 852–857 (2012).
21. K. Waltar, J. Haase, M. Lucchini, J. A. van Bokhoven, M. Hengsberger, J. Osterwalder, and L. Castiglioni, "Polarization-sensitive pulse reconstruction by momentum-resolved photoelectron streaking," Opt. Express **26**, 8364–8374 (2018).
22. M. Gensch, L. Bittner, A. Chesnov, H. Delsim-Hashemi, M. Drescher, B. Faatz, J. Feldhaus, U. Fruehling, G. Geloni, C. Gerth, O. Grimm, U. Hahn, M. Hesse, S. Kapitzki, V. Kocharyan, O. Kozlov, E. Matyushevsky, N. Morozov, D. Petrov, E. Ploenjes, M. Roehling, J. Rossbach, E. Saldin, B. Schmidt, P. Schmueser, E. Schneidmiller, E. Syresin, A. Willner, and M. Yurkov, "New infrared undulator beamline at flash," Infrared Phys. Technol. **51**, 423–425 (2008).
23. C. Bellei, J. R. Davies, P. K. Chauhan, and Z. Najmudin, "Coherent transition radiation in relativistic laser-solid interactions," Plasma Phys. Controlled Fusion **54**, 035011 (2012).
24. K. Tiedtke, A. Azima, N. von Bargen, L. Bittner, S. Bonfigt, S. Düsterer, B. Faatz, U. Frühling, M. Gensch, C. Gerth, N. Guerassimova, U. Hahn, T. Hans, M. Hesse, K. Honkavaar, U. Jastrow, P. Juranic, S. Kapitzki, B. Keitel, T. Kracht, M. Kuhlmann, W. B. Li, M. Martins, T. Núñez, E. Plönjes, H. Redlin, E. L. Saldin, E. A. Schneidmiller, J. R. Schneider, S. Schreiber, N. Stojanovic, F. Tavella, S. Toleikis, R. Treusch, H. Weigelt, M. Wellhöfer, H. Wabnitz, M. V. Yurkov, and J. Feldhaus, "The soft x-ray free-electron laser flash at desy: beamlines, diagnostics and end-stations," New J. Phys. **11**, 023029 (2009).
25. G. Geloni, V. Kocharyan, E. Saldin, E. Schneidmiller, and M. Yurkov, "Theory of edge radiation. Part I: Foundations and basic applications," Nucl. Instrum. Methods Phys. Res. A **605**, 409–429 (2009).
26. M. Walther, D. G. Cooke, C. Sherstan, M. Hajar, M. R. Freeman, and F. A. Hegmann, "Terahertz conductivity of thin gold films at the metal-insulator percolation transition," Phys. Rev. B **76**, 1–9 (2007).
27. J. Schötz, B. Förg, M. Förster, W. A. Okell, M. I. Stockman, F. Krausz, P. Hommelhoff, and M. F. Kling, "Reconstruction of nanoscale near fields by attosecond streaking," IEEE J. Sel. Top. Quantum Electron. **23**, 77–87 (2017).
28. B. Förg, J. Schötz, F. Süßmann, M. Förster, M. Krüger, B. Ahn, W. A. Okell, K. Wintersperger, S. Zherebtsov, A. Guggenmos, V. Pervak, A. Kessel, S. A. Trushin, A. M. Azzeer, M. I. Stockman, D. Kim, F. Krausz, P. Hommelhoff, and M. F. Kling, "Attosecond nanoscale near-field sampling," Nat. Commun. **7**, 11717EP (2016).
29. B. Rösner, P. Dudin, J. Bosgra, M. Hoesch, and C. David, "Zone plates for angle-resolved photoelectron spectroscopy providing sub-micrometre resolution in the extreme ultraviolet regime," J. Synchrotron Radiat. **26**, 467–472 (2019).
30. K. Medjanik, O. Fedchenko, S. Chernov, D. Kutnyakhov, M. Ellguth, A. Oelsner, B. Schönhense, T. R. F. Peixoto, P. Lutz, C. H. Min, F. Reinert, S. Däster, Y. Acremann, J. Viefhaus, W. Wurth, H. J. Elmers, and G. Schönhense, "Direct 3D mapping of the Fermi surface and Fermi velocity," Nat. Mater. **16**, 615 (2017).